International Journal of Scientific Research in Science and Technology
Print ISSN: 2395-6011 | Online ISSN: 2395-602X (www.ijsrst.com)
doi : https://doi.org/10.32628/IJSRST

Investigative Analysis on Mechanical Properties of Laser-Sintered-Nylon Diamond Lattices

S. Lingamaiah

M.Tech, Head of the Mechanical Engineering Department and Assistant Professor, S. K. University College of Engineering and technology, Ananthapuramu, Andhra Pradesh, India

Article Info
Volume 8, Issue 6
Page Number : 178-199

Publication Issue
November-December-2021

Article History
Accepted : 05 Nov 2021
Published : 14 Nov 2021

ABSTRACT

Additive manufacturing offers a manufacturing technique to produce complex geometry prototypes at a rapid pace and low cost. These advantages advocate additive manufacturing for the design and production of cellular structures. Cellular structures are interesting because they contain a large amount of porosity (void space of air) to manifest a lightweight structure. Designs of cellular structures generate a periodic pattern; often of complex geometry, called a lattice. The research involves PA2200 (Nylon 12) laser sintered diamond lattices with experimental compression testing and direct FEA model comparison. A correction factor is applied for a design offset of laser sintered lattices. Once applied, the experimental and FEA data agree in validating the diamond lattice as a bending-dominated structure. Diamond lattices show a 4^{th} order relationship between stiffness and parameters of thickness and unit cell length. For density, stiffness maintains a 2^{nd} order relationship, as predicted by bending dominated structures. The resulting stiffness can be tuned over a stiffness range of four orders of magnitude. Further research shows the results for modifying the diamond lattice and scaling stiffness and density using other materials (like metals) to expand the range of stiffness and compare diamond lattices on material property charts. Lastly, the effective Poisson's ratio varies from 0.5 to 0.4 depending on the *(t/L)* ratio.

Keywords : Buzz News, Dropout layer, Fake news, Long Short Term Network Model, Social media

I. I.INTRODUCTION TO CELLULAR MATERIALS BACKGROUND

Materials containing significant void space –termed porosity-throughout a given volume are termed cellular solids. It is the dispersion of pores throughout a solid that yields a porous material. Cellular solids are a sector of materials that is often overlooked for finer details in terms of mechanical aspects such as: stiffness, density, and strength. However, if one observes closely, one finds numerous cellular materials such as: meshes, foams, and micro-lattices-

both natural and synthetic. To the average person, cellular materials take the form of foams for packaging or cushions that are compliant and energy absorbent. In the culinary profession, cellular solids present themselves in the form of foods that are not fully dense, such as: bread and cakes or even a spongy mousse. Cancellous bone and wood are also natural cellular materials. Since cellular means a material containing porosity, an engineer can take advantage of using cellular materials, which present unique balances of properties. For example, lightweight structural elements having the capabilities of tuning stiffness and density while also having potential for energy absorbance. Multi-functionality is a potential benefit of cellular solids if multiple applications are required.

ADDITIVE MANUFACTURING (AM) BACKGROUND

AM is defined exactly as the name suggests; primarily an *additive* process as it builds a part by the addition of material layer-by-layer. There are a variety of production methods of 3D printing using the additive term including Fused Deposition Modeling (FDM), Laser Sintering or Melting, and even binder jetting technologies. All of which start constructing a part from a base layer of material and then add layers that are combined together by the means tailored to the individual AM process (thermoplastic adhesion, laser sintering, and binder gluing).

A fundamental advantage of AM is the speed at which the process of manufacturing a part occurs relative to traditional manufacturing techniques. AM is much quicker in generating a part from start to finish, thus appropriately nicknamed “rapid prototyping”. The quicker process is accelerated by taking a CAD model and directly manufacturing a prototype or part. In traditional manufacturing methods, often a prototype needs several processes to be completed and could go through several people each with a different skill to implement their manufacturing expertise.

Conventional manufacturing methods such as casting, injection molding or machining, etc. entail part-specific tooling. Part-specific tooling of fixtures and other tools specific to the manufacturing of a specific prototype or part, generate extra cost for the initial build of a part. Since there is an initial cost, the first part is much more expensive than the tenth or hundredth part. Additive manufacturing doesn’t require part specific tooling so the first part costs the same as the hundredth part.

PREVIOUSLY RESEARCHED FOAMS AND LATTICE STRUCTURES

Meta-materials have been investigated in both stochastic and periodic, ordered lattice structures. Stochastic meta-materials are foams possessing unpredictability throughout the interior of the structure. The exterior skeleton is often defined by a mold to capture the overall shape. However, the interior is stochastic as the foam expansion is frequently processed by the use of a foaming agent, heat, and pressure to expand the material. Since a foaming agent is used the interior is unpredictable to a certain extent as the interior spacing, size, and location of the porous features is not exact. An example of a stochastic foam is presented in Figure 1.3a to show the unpredictability of the interior features for the cellular system.

The design and topology of metal foams is presented in an extensive design guide by Ashby, in order to fabricate and characterize metal foams with open or closed cells. To further characterize stochastic foams, research has been conducted to analyze the deformation characteristics for energy absorbing applications and the cyclic properties of open and closed cell foams. A unique approach to fabricating metal foams was done by Murr utilizing conversion of

aluminum foam CT scans to create stochastic foams by the AM process of Electron Beam Melting (EBM). Since foams are highly irregular, the stochastic nature will need to be evaluated for the direction of loading as the chance of being isotropic is very unlikely. To understand this behavior, anisotropy of foams was studied by Huber,

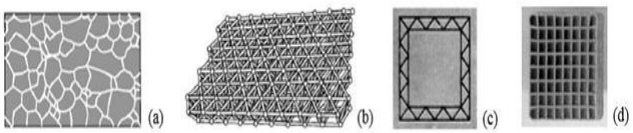

Cellular systems: stochastic (a) , periodic (b) and 2D extruded prismatic metals: mesh in between outer and internal diameter (c) , internal mesh with solid outer diameter exoskeleton (d)

Along with the development of AM, the rise of design space research for meta-materials in the form of repeating lattice structures has also increased. Figure 1.3b is representative of a 3D cellular structure possessing long range, repeated order. As previously mentioned, AM provides a production technique to fabricate 3D meta-materials allowing lattice structures of complex geometry to be prototyped allowing the evaluation of mechanical properties. Here, a lattice is defined as a network of connected struts with a defined periodic geometry. For lattice structures, the goal of lattice design is to design lightweight structures with valuable combinations of properties such as rigidity, flexibility, compliancy, and energy absorbance with the capability of tailoring mechanical properties such as: elastic modulus, density, and Poisson's ratio. This is achieved across a wide range of properties by varying the building parameters that directly affect the relative density of the lattice. By utilizing a minimal amount of material, the lattice structure has low density, thus yielding a cellular solid with high porosity. Examples of complex geometries manufactured by AM include a 3D re-entrant dodecahedron with auxetic behavior (negative Poisson's ratio). In order to investigate highly structural efficient stretch dominated lattice structures, unit cells in the topology of octet trusses and gyroids have been designed and tested to examine the effect on mechanical properties by changing unit cell length. Octet lattice structures have Face-Centered-Cubic (FCC) topology resulting in high stiffness. Also, the deformation and failure behavior of Body-Centered-Cubic (BCC) unit cells was characterized by Gorny, Figure 1.4 illustrates the complexity of shape for the different cellular lattices and why the AM is utilized as the manufacturing strategy to research the characteristics of cellular systems. The above mentioned unit cells, kagome lattices, and pyramidal lattices have had significant research to evaluate high elastic modulus lattice structures seeking to maximize stiffness; however, much less research has been completed on low stiffness structures.

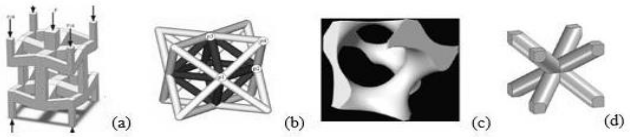

3D cellular structure unit cells: re-entrant dodecahedron (a), octet (b), gyroid (c), BCC (d)

DIAMOND LATTICE STRUCTURE AND TOPOLOGY

Molecular configuration of diamond has a unique FCC unit cell encompassing eight carbon atoms. To understand the topology of the diamond unit cell, Figure 1.5 illustrates the molecular structure for a diamond unit cell where two interpenetrating FCC lattices are offset by a quarter diagonal from the coordinates (0,0,0,) to (1/4, ¼, 1/4). Another noteworthy characteristic pertaining to Figure 1.5 is all inter atomic connections are of equal length in every direction.

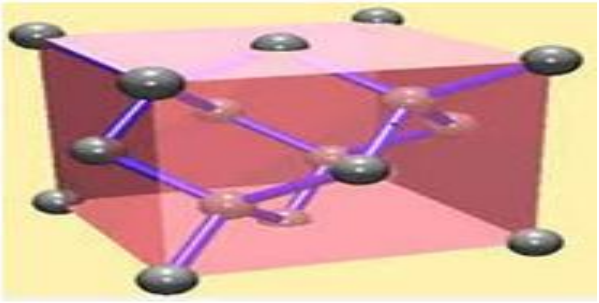

Diamond lattice molecular unit cell

In designing an additive manufactured lattice structure based on the diamond lattice configuration, the atom centers become lattice nodes. Each node is connected to four other struts that connect to the other nodes within the unit cell, Figure 1.6 displays Finite Element Analysis (FEA) models of the unit cell configuration for diamond. An aspect to observe in Figure 1.6 is the wide, sweeping tetrahedral angles of 109.5°. These obtuse angles are the core indication to hypothesize the lattice structure to be flexible and compliant. This is derived from the reasoning that as a compressive force is applied to the diamond lattice, the broad angles will allow bending between tetrahedral struts producing a flexible and compliant structure. Having properties of flexibility implies energy can be absorbed and suggests the topology of diamond has potential to fill meta-material design space with bending dominated, low stiffness structures of low density.

To describe the diamond lattice, build parameters are introduced in Figure 1.6. The unit cell length *(L)* is the dimension from the top to bottom surface of the unit cell. The thickness *(t)* is the cross section thickness considering the primary bending direction of a vertical load. The other cross section thickness *(w)* was set to *1.25t* to strengthen the lattice in the horizontal orientation to assure bending to be consistent about the vertical axis.

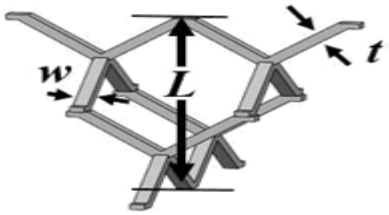

Model for the unit cell structure of diamond

II. FOUNDATION OF CELLULAR MATERIALS

An broad foundation has been provided by Ashby for characterizing cellular materials as meta-materials. The goal of creating meta-materials is to provide a lattice structure that is a lightweight, load bearing structure with potential secondary functions of energy absorbance, thermal dissipation, etc.

Here, it is important to differentiate between open and closed cell lattices. Open cell lattices like those of Figure 2.1 have an open faces for the boundary of the unit cell. Closed cell lattices similar to Figure 2.2 have a sheath or a film that encloses the unit cell of the structure. With this sheath sealing the unit cell of the lattice, the complexity of closed cell mechanical property equations increases. Stretching of the sheath (face stretching) and compression of the gas/liquid within the unit cell complicates the mechanics of closed cell lattices. Imagine as the closed cell lattice is compressed, the face sheath is stretched in the direction perpendicular to the applied force. Upon stretching the sheath, the reaction must be accounted for in the property equations. Since the closed cell lattice has a gas or liquid trapped in the unit cell, compression of the enclosed fluid should also be accounted for when deriving the equations. However, if the thickness of the sheath ( ) is much less than the thickness of the strut and also a material with less mechanical strength or the surrounding pressure is equal to atmospheric pressure, then both effects can be regarded as negligible. Typically most lattice structures researched are open cell as they are simpler to 14 manufacture and analyze. Throughout the

remainder of the thesis all following equations and analysis are for open cell lattices.

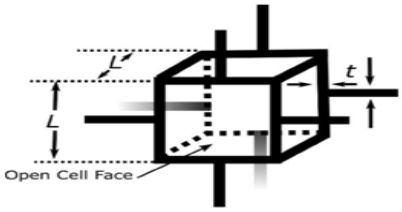

Figure 2.1: Open cell lattice

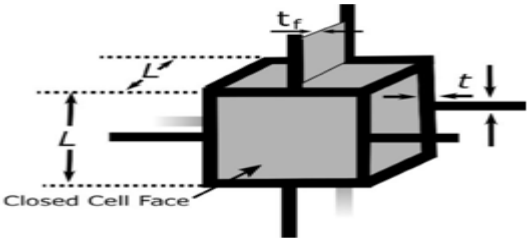

Closed cell lattice

GOVERNING PRINCIPLES OF CELLULAR LATTICE MATERIALS

There are three principles that govern the properties of cellular lattice materials. Figure 2.3 below illustrates the governing principles of cell topology and shape, material, and relative density in a flowchart. Each principle is then broken down into sub-categories to describe each principle in further detail.

Cell Topology and Shape

Upon designing a lattice topology and shape, many aspects of the structural behavior are set. Cellular lattices are categorized into either stretch or bending dominated structures. Bending dominated lattices are distinguished by properties of flexibility and compliance for energy absorbance, yet a lower to moderate strength. Stretch dominated lattices are much more structural efficient but sacrifice any sort of compliance. As compliance is diminished, the lattice can no longer absorb energy.

Maxwell's criterion relates the geometric connections of the structure to the mechanical behavior of the lattice as being more stretch-dominated or bending-dominated. Maxwell's criterion is given by:

$$M = b - 2j + 3 \; ; \; (2D)$$
$$M = b - 3j + 6 \; ; \; (3D) \qquad \text{Equation 1}$$

where *(b)* represents the number of struts and *(j)* being the number of joints. Therefore lattice structures are split up in two divisions: one being bending dominated behavior and the other stretch dominated. If $M < 0$; the lattice structure will be governed by bending dominated behavior. Conversely, when $M \geq 0$; the meta-material lies in the stretch dominated regime.

Figure 2.4a below displays a bending dominated mechanism if the joints are bonded together. When a compressive force is applied the struts endure deformation and deflection and yield by bending. Its counterpart Figure 2.4b, however, will not bend because it has a support strut across the middle of the mechanism. Now when a compressive force is applied to the mechanism, the center crossbar is "stretched". This enables stretch dominated lattices to be much stiffer as the elements now bear tensile loads, thus increasing the strength. A stretch dominated lattice is presented in Figure 2.5. Since there are multiple struts combining into one joint, Maxwell's equation calculates to $M = 18$ to clearly define Figure 2.5 as a stretch dominated lattice. When a compressive force is applied to the lattice in Figure 2.5, the struts will be in either tension or compression creating a high strength lattice. This lattice also characterizes meta-material structures precisely as the mechanical response will be unique when placed in loading conditions.

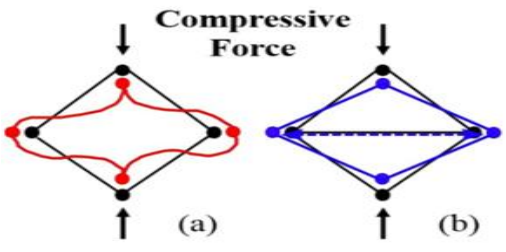

Example of bending (a) vs stretch (b) dominated behavior with deformation after compressive force

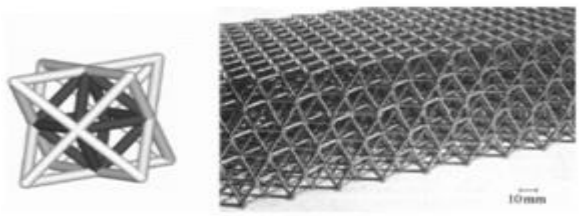

Example of stretch dominated lattice

Relative Density

The relative density is a key principle because it has a major influence on effective mechanical properties of a lattice structure through the determination of thickness *(t)* and repeating unit cell length *(L)* seen in the open cell lattice of Figure 2.1. Thickness *(t)* is defined by the width of the struts and unit cell length *(L)* characterized by the distance from the top to bottom strut of the unit cell As the thickness *(t)* is increased or the unit cell length *(L)* is decreased, the lattice material will occupy an increased amount of volume within the unit cell of a lattice structure. As the volume of material increases within a unit cell, the density will also increase. Oppositely, if the thickness *(t)* is decreased or the unit cell length *(L)* is increased, the material will occupy a decreased amount of volume thus decreasing the density of the lattice structure. Manipulation of the density directly effects the mechanical properties, these relationships will be derived and analyzed in later sections.

BENDING DOMINATED BEHAVIOR

As mentioned previously, bending dominated lattices have mechanical properties consisting of compliance and flexibility, yet a moderate to low stiffness. The structure in Figure 2.4a can only resist deflection due to the fact that the actual parts do not have pin joints but rigid bonds. When a force is applied, the members bend. This is advantageous in applications especially requiring energy absorbance where flexibility and compliance are crucial.

Bending Dominated Relative Density vs Relative Elastic Modulus Derivation

Most open cell lattice structures will have more complex topology than the simple example in Figure 2.1. However, if the lattices deform and fail by the same mechanisms, then the mechanical properties can be understood using dimensional arguments which omit all constants arising from the specific cell geometry. For bending dominated structures, the relative density is defined by a squared relationship of *t/L* below in Equation 2 :

$$\frac{\rho^*}{\rho_{bulk}} \propto \left(\frac{t}{L}\right)^2 \qquad \text{Equation 2}$$

The relative density is termed the effective density of the lattice (ρ^*) divided by the bulk material density (ρ_{bulk}). If the cross section is scaled uniformly, the second moment of area is proportional to the characteristic cross section dimension t raised to the fourth power, ($I \propto t4$). Moreover, standard beam theory suggest that deflection (δ) is proportional to properties of Equation 3, where elastic modulus (E) is the modulus of bulk material. Deflection (δ) is demonstrated in Figure 2.6 to illustrate how the lattice will deflect.

$$\delta \propto \frac{FL^3}{E_{bulk}I} \qquad \text{Equation 3}$$

Also considering the conventional stress and strain relationships of: $\sigma \propto F/L2$ and $\varepsilon \propto \delta/L$ to combine with Equation 3 yields Equation 4.

$$E^* \propto \frac{\sigma}{\varepsilon} \propto \frac{E_{bulk}I}{L^4} \qquad \text{Equation 4}$$

By substituting the second moment of area equation ($I \propto t4$) into Equation 4, Equation 5 is derived to directly relate relative elastic modulus and relative density for bending dominated structures where ($E*$) and ($\rho*$) are effective modulus and density pertaining to an individual lattice.

$$\frac{E^*}{E_{bulk}} \propto \left(\frac{\rho^*}{\rho_{bulk}}\right)^2 \qquad \text{Equation 5}$$

Relative stiffness can be represented in another equation involving thickness *(t)* and unit cell length *(L)* by substituting the relative density relation of Equation 2 into Equation 5 to give Equation 6 below. The relationship of *(t/L)* to relative stiffness is to the fourth power, so modifying *(t)* or *(L)* will change relative stiffness significantly.

$$\frac{E^*}{E_{bulk}} \propto \left(\frac{t}{L}\right)^4 \qquad \text{Equation 6}$$

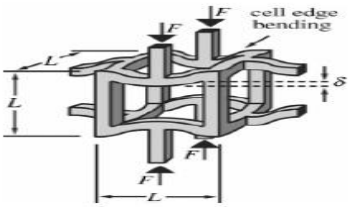

Bending dominated structure under applied force (*F*) with deflection *(δ)*

Bending Dominated Deformation Characteristics and Derivation

As formerly stated, bending dominated lattices have flexibility. Thus, bending dominated structures absorb energy much more effectively that stretch dominated structures. Observing Figure 2.7, a stress-versus-strain curve for bending (red) and stretch (blue) dominated structures typically shows the following trend of stress for increasing strain.

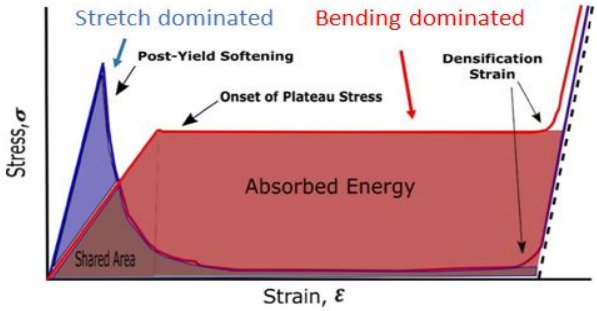

Stress vs strain for bending and stretch dominated structures

Three regimes of deformation occur for bending dominated structures as illustrated in Figure 2.7. The first is the linear elastic portion of the curve. In this region the main deformation is concerned with bending of the lattice struts. Next is the plateau stress of the lattice where the onset of cell collapse by yielding, bucking, and crushing will ensue. Following the plateau stress is the last region of densification where a sharp increase in stress takes place as the lattice structure is collapsed so that the cell struts are now in contact with each other. The feature to be highlighted from this curve is the plateau stress at which as the stress is nearly constant for a wide range of increased strain. Over this strain area, the lattice is bending and collapsing to absorb the energy applied to the lattice. The area under the stress-vs-strain curve is significantly greater for bending dominated lattices, thus permitting much more energy absorbance. Bending dominated lattices excel in energy absorbance and impact resistant structures. The plateau stress ($\sigma plat$) can be derived in the following manner: cell walls start to yield when the force exerted on them exceeds their fully plastic moment of Equation 7 below with being the yield strength of bulk material the lattice is constructed of.

$$M \propto \left(\frac{\sigma_{bulk} t^3}{4}\right) \qquad \text{Equation 7}$$

The moment from Equation 7 is related to stress in the conventional form of Equation 8:

$$M \propto FL \propto \sigma L^3 \qquad \text{Equation 8}$$

By inserting Equation 7 into Equation 8, and remembering Equation 2 is the thickness divided by unit cell length (t/L) proportional to the square root of relative density derives Equation 9 for the relative strength of a bending dominated lattice, where the plateau stress ( ) level can be found.

$$\frac{\sigma_{plat}}{\sigma_{bulk}} \propto \frac{1}{4}\left(\frac{\rho^*}{\rho_{bulk}}\right)^{3/2} \qquad \text{Equation 9}$$

At the point of the plateau stress($\sigma plat$), three failure modes of: plastic yielding/bending, elastic buckling, or collapse by brittle fracture compete. The failure mechanism that requires the lowest stress will prevail in failure. For bending dominated lattices made of

ductile materials, the most likely mode of failure will be the onset of plastic yielding and bending at the unit cell boundaries. Figure 2.8a illustrates plastic yielding of the corners of the unit cell. Plastic yielding is the failure mode allowing the longest plateau stress to be reached because the lattice will keep bending until the densification strain is reached. As the lattice is enduring increasing strain, thus further and further plastically deformed, the stress is held constant to absorb energy over the greatest amount of area. Elastomeric lattice materials like rubber fail by buckling (Figure 2.8b). Also the larger the slenderness ratio *(t/L)* of the struts, the greater chance of buckling due to the fact of a larger slenderness ratio reduces the Euler buckling load.Brittle lattices have the smallest region of plateau stress. Ceramic lattices are an example of brittle fracture failure and collapse by successive fracturing of the unit cell, initialized in Figure 2.8c. An extended plateau stress region is preferred for bending dominated lattices, therefore the more ductile the material chosen will generate higher energy absorption through more.

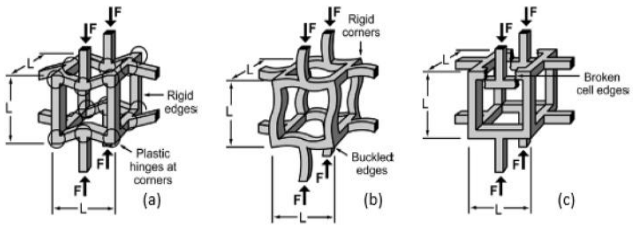

Bending dominated failure modes; (a) plastic bending (b) buckling (c) brittle fracture

STRETCH DOMINATED BEHAVIOR

Unlike bending dominated, stretch dominated structures are designed for high structural efficiency. High structural efficiency is aimed to maximize the specific stiffness and strength ratio. This is accomplished by constructing a lattice to have significantly high stiffness and strength, yet keeping in mind the centralized goal of minimum material through low relative density. A stretch dominated lattice generates high stiffness and strength through the means of having added supports in a unit cell. Figure 2.4b represents these additional supports now carrying tension or compression depending on the loading. As mention previously, as Figure 2.4b is loaded in compression, the middle crossbar is now placed in a state of tension, thus implying the "stretch". Once a support is in a state of tension, the stiffness and strength sharply increases due to the fact that slender structures are much stiffer when stretched than when bent and/or compressed.

Stretch dominated lattices first respond by elastic stretching of its struts. For stretch dominated lattices, an average of one third of its struts carry tension when the structure is loaded in simple tension. Through the same approach as bending dominated lattices, stretch dominated structures derive a relationship for relative density and elastic modulus of Equation 10 below.

Equation 10 presents a linear relationship of relative stiffness to relative density for stretch dominated structures. A linear relationship (power of one) makes stretch dominated lattice stiffer by of a factor of 3-10 for the same relative density of a bending dominated lattice (power of two).

$$\frac{E^*}{E_{bulk}} \propto \frac{1}{3}\left(\frac{\rho^*}{\rho_{bulk}}\right) \qquad \text{Equation 10}$$

Figure 2.7 depicts the stress versus strain behavior of stretch dominated lattices where a plateau stress is no longer evident like that of a bending dominated structure. Without any plateau stress, the area is much less under the stretch dominated stress-vs-strain curve; thus having much less capability of energy absorbance. Stretch dominated structures fail first by the onset of plastic deformation by stretching. The next response is post-yield softening after the initial yield, plastically buckling, or brittle collapse of the struts follows. Post-yield softening consists of a severe decrease in stress as strain is further increased

past the initial yield. With the action of post-yield softening, stretch dominated structures are not ideal candidates for energy absorbing applications as a flat plateau stress is desired. The last regime of failure is same as bending dominated for densification of the lattice. The key takeaway for stretch dominated lattices is that both the modulus and initial collapse strength are much higher than bending dominated, suiting them for lightweight structural applications requiring high specific stiffness and strength.

POTENTIAL DESIGN SPACE FOR LATTICE STRUCTURES

An interesting approach for lattice structures is to plot the relative modulus versus relative density. Figure 2.9a and Figure 2.9b compare bending dominated to stretch dominated behavior with the relationship of relative modulus and strength to relative density with a few existing researched cellular structures. The slopes of the curves; 2 for bending dominated and 1 for stretch, on a log-log plot are applied from the relative modulus and strength limits. From the upper bound, bending dominated structures decrease in modulus more rapidly with a quadratic relationship. This reinforces the idea of stretch dominated lattice being stiffer by a factor of 3-10 (for the cellular solids/lattices relative density range), approaching 10 as the relative density is decreased further and is observed when compared in Figure 2.9

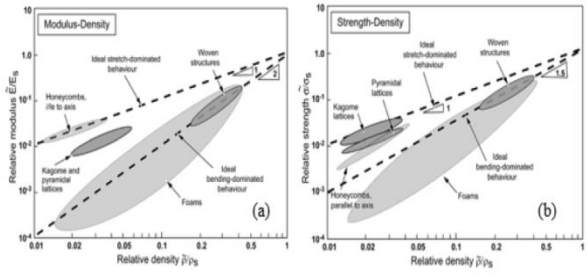

Relative modulus vs relative density (a) and relative strength vs relative density (b)

Ideal bending dominated behavior slices right through the area of foams, confirming that bending dominated structures will behave as energy absorbers similar to foams. Foams envelope such a wide area outside of the ideal bending line because many foams heterogeneous structures. Because foams are stochastic, strong and weak zones exist causing the stiffness to fluctuate, resulting in the wide area. 2D honeycombs lie on the ideal stretch line. This is due to the exceptional structural efficiency of honeycombs when loaded parallel to its hexagonal axis. Other researched lattices of Kagome and pyramidal lattices are slightly below ideal stretch behavior. It is encouraging to observe 3D lattice structures have the potential to fill voids on the relative stiffness versus relative density chart. The potential to fulfill unoccupied areas of stiffness versus density is the baseline motivation for cellular meta-materials and the reason current research is being conducted.

III. DIAMOND LATTICE NUMERICAL STUDIES AND EXPERIMENTAL COMPARISON

DIAMOND LATTICE BUILD PARAMETER DETAILS

To explore how the diamond lattice would change mechanical properties, a wide range of unit cell lengths and thicknesses were manufactured through Laser Sintering (LS) and also analyzed in FEA. Unit cell lengths *(L)* were modified from 5 – 20 millimeters and thickness of the struts *(t)* varied from 0.5 – 2 millimeters, both parameters shown in Figure 1.6.

In order to understand how the parameters of unit cell length *(L)* and element thickness *(t)* vary the configuration of the diamond lattice, hence, directly the effective density of a combination of unit cell length *(L)* and thickness *(t)*, Solidworks models are rendered below. All of the laser-sintered diamond lattices and Solidworks models were (2x2x2) arrays of unit cells except where noted. As previously mentioned, the thickness *(t)* is the cross section thickness in the primary bending direction under a

vertical load. The other cross section dimension *(w)* was set to 1.25*t* to assure bending about a consistent axis. Figure 3.1 portrays the effect of thickness for a constant unit cell length of 10 mm. As the thickness is increased from 0.5 -2 mm, the relative density of a diamond lattice with a 10 mm unit cell length increases significantly from 2.15 to 27.55 %.

When the thickness is held constant while varying unit cell length, relative density is changed in an inverse proportion. Figure 3.2 below shows a constant 1 mm thickness and varying the unit cell length from 5 – 20 mm. As the unit cell length increases, the relative density decreases because increasing the distance from top to bottom of the unit cell makes the thickness of the struts proportionally smaller as seen below. It is worthy here to note the effect of relative density by adjusting the unit cell length and thickness for the reason that it directly affects the mechanical response of the diamond lattice.

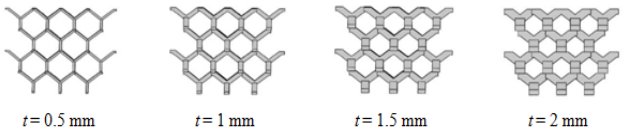

Variation of element thickness *(t)* for unit cell length *(L)* of 10 mm

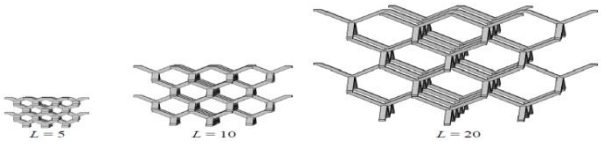

Variation of unit cell length *(L)* for constant element thickness *(t)* of 1 mm

IV. Experimental Research Method

Diamond lattice samples consisting of 2x2x2 arrays of diamond lattice cells were fabricated on an EOS Formiga P100 from PA2200 powder (50% virgin, 50% recycled) with a powderbed temperature of 170 C using 0.100 mm layers and 0.25 mm scan spacing. Scan speeds were 2500 mm/s on hatching and 1500 mm/s on the edges using 21W and 16W respectively. All parts were printed in the XYZ orientation as defined in ASTM F291-11. Parts were positioned at least 45 mm from the edges of the build volume and allowed to cool overnight before removal from the powder bed. The parts were cleaned with compressed air. Compression testing was performed on a Tinius Olsen Model H5K-S UTM 5kN testing system using the axis motion to calculate the applied strain. The displacement rate was adjusted to maintain a constant strain rate of 5%/min for all samples. Three to five samples were tested for each condition.

A schematic of laser sintering process is shown below in Figure 3.3 and summarized in the following. Laser sintering systems lay down a layer of powder leveled by a roller in a heated build chamber just below the melting point and/or glass transition temperature of the powdered material. Once the roller levels the powder, cross-sectional sintering or fusion of the powder particles takes place by a $_2$ laser in the geometry digitally controlled. The surrounding powder that isn't thermally fused acts as support for following layers so the need for additional supports is eradicated. The process repeats with additional layers of powder by lowering the build platform by one layer thickness and laser sintering of the specified geometry until the part is finished from the base to top layer.

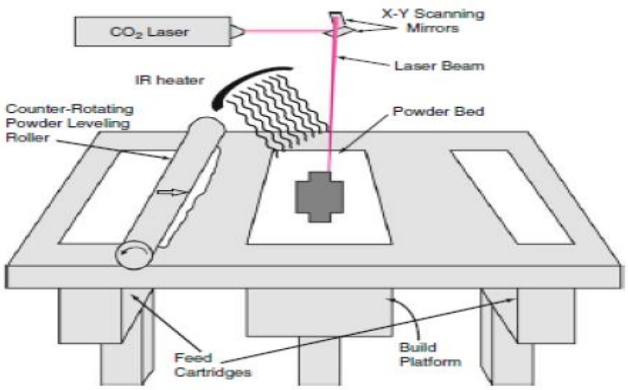

Laser sintering process

FEA SIMULATION METHOD

The compression tests were simulated using finite element analysis (FEA) in SolidWorks. Boundary conditions were chosen to model the experimental

compression testing with a fixed lower platen of a compression tester with an applied displacement on the top as illustrated in Figure 3.4 below. For the simulation, the diamond lattice's bottom pads were set to a zero displacement in the z-direction. The bottom center contact point was fixed in all directions. This enabled the other bottom pads to slide in the x and y directions to accommodate transverse displacements. Motion in the x and y direction of bottom pads is characterized as "slipping" meaning the bottom pads would translate horizontally on a bottom plane as the diamond lattice is compressed. The top pads (seen in Figure 3.4 below) were set to a fixed displacement in the z-direction. A fixed displacement *(δ)* was set to simulate a certain desired strain for compression of the diamond lattices. For example, if the unit cell length of 10 mm (height of 20 mm for 2x2x2 array) was displaced 1 mm, this created an effective strain of 5%. The manufacturer supplied bulk properties values for Nylon (PA 2200: 1.7 GPa for modulus, 0.394 for Poisson's ratio, and 930 kg/m^3) were used for the material properties in the simulation. Ahmadi and Campoli both support similar methods of FEA for evaluating properties of open cell porous structures.

A mesh convergence study was conducted for the various unit cell lengths and thickness combination to ensure refinement of the mesh was sufficient to have less than 1-2 % change in reaction forces when halving the element size. Large deflection conditions (Non-Linear Simulation) produced no more than 0.84 – 1.5 % deviation as compared with linear analysis for 1% applied strains so linear results at 1% applied strains were used for all effective elastic modulus results reported below.

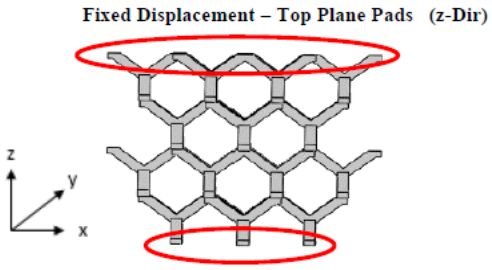

Boundary conditions for simulating compression testing of diamond lattice

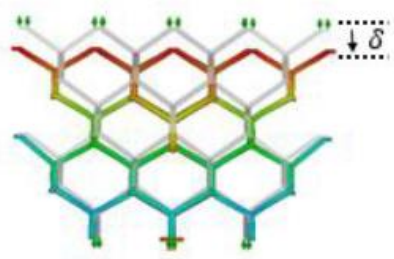

Plot of z displacements in a simulated diamond lattice under an applied displacement of *(δ)*.

Representative resulting diamond lattice deformations are illustrated above in Figure 3.5 with an applied displacement of *(δ)*. The resultant force on the bottom pads was extracted to estimate the force of compression. After the resultant force was extracted it was converted to stress as the resultant force over the bottom plane area; the stress divided by the applied strain value produced an effective elastic modulus(E^*).

Additional simulations were performed to determine whether the compression stiffness of the 2x2x2 arrays of unit cells is representative of the bulk properties of 4x4x4 and 6x6x6 unit cell arrays with many more unit cells *(N)* as illustrated in Figure 3.6. The 4x4x4 and 6x6x6 models were cut into quarter models in an effort to reduce simulation run time meanwhile obtaining accurate values of stiffness. Then symmetry conditions were applied to the quarter models (example of original and sliced 4x4x4 lattice shown in Figure 3.7 & Figure 3.8 below along with the same zero and fixed displacements as previously applied.

Now however, the absolute fixed point was at the intersection of the two symmetry planes.

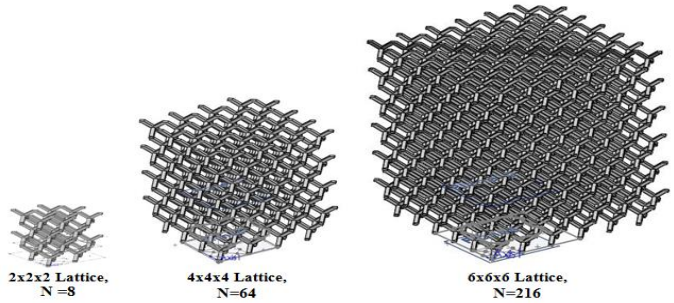

Diamond lattices with different numbers of unit cells

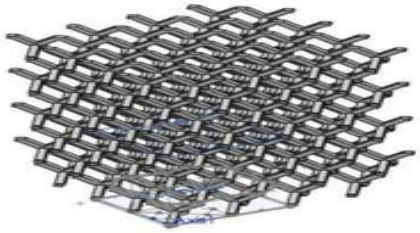

Original 4x4x4 lattice

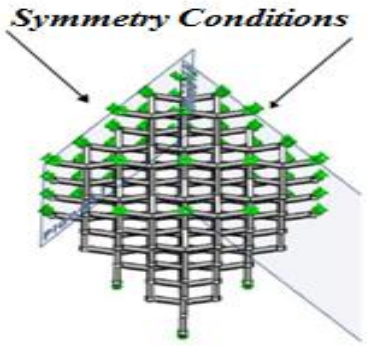

Simplified 4x4x4 unit cell diamond lattice model after applying symmetry conditions

The stiffness of the larger models was calculated as before and compared to the 2x2x2 unit cell values. Figure 3.9 compares the relative stiffness on a log-log scale for the different number of unit cell lattices studied. Observing Figure 3.9 shows the relative stiffness fluctuates only slightly (~5%) and maintains a close to constant line for the different combinations of *(t)* and *(L).*

The change of elastic modulus has a max of 7% with most points floating between 4 – 6 % and the error from using the smaller test sample (2x2x2 unit cells) is minimal compared to the modulus variation of over 1000x across the geometries studied.

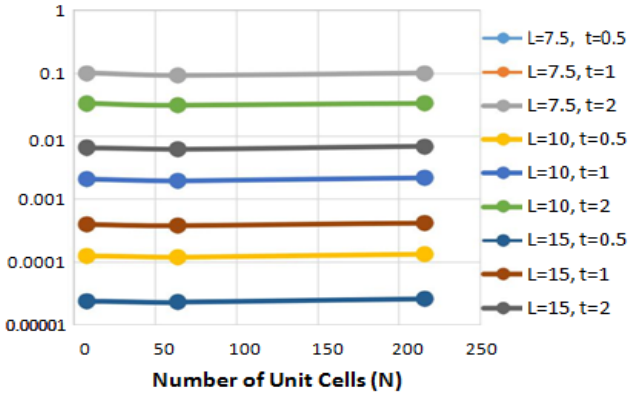

Relative stiffness study for different number of unit cell lattices

V. EXPERIMENTAL VS FEA RESULTS

The range of lattice conditions used in the simulations and in experiments are summarized in Table 1. Simulation results predict a change of elastic modulus proportional to the power of four for a given thickness and unit cell length. These trends are presented in Figure 3.10 and Figure 3.11 below. The approximate fourth power relationship (varying from 3.83 – 4.07) with most of the exponents existing in the range of: 4 +/- 0.04.The fourth power relationship supports the assertion that diamond lattices are bending dominated structure, recall Equation 6 is the derivation of effective stiffness (elastic modulus) as a proportional fourth power relationship between thickness *(t)* and unit cell length *(L).*The results can be condensed to a relationship between the effective modulus and the ratio of element thickness to unit cell length *(t/L).* This relationship is represented in Figure 3.12 below. A special note for the *(t/L)* ratio, the cellular solids relative density limit of 30% equates to a *(t/L)* value of 0.2 As *(t/L)* increases, both the density and the stiffness increase as well. Since a thickness/length ratio *(t/L)* can be achieved with various combinations of unit cell length and thickness, other considerations such as process accuracy, build

time can be utilized to select the specific parameters used to obtain to generate a diamond lattice for a specific application.

Table 1 : Range of FEA and experimental stiffness for size parameters

Unit Cell Length *(L)* [mm]	Thickness *(t)* [mm]	*(t/L)*	FEA Simulation Eeff (MPa)	Experimentally Measured Eeff (MPa) with St. Dev.
5.0	0.5	0.100	3.59	0.504 ± 0.013
5.0	1.0	0.200	56.77	21.37 ± 0.483
5.0	1.5	0.300	263.51	N/A
5.0	2.0	0.400	708.33	N/A
7.5	0.5	0.067	0.69	0.099 ± 0.016
7.5	1.0	0.133	11.29	N/A
7.5	1.5	0.200	56.27	N/A
7.5	2.0	0.267	169.54	N/A
10	0.5	0.050	0.21	0.040 ± 0.0004
10	1.0	0.100	3.51	1.56 ±0.010
10	1.5	0.150	17.97	10.93 ± 0.521
10	2.0	0.200	55.98	29.77 ± 1.585
12	0.5	0.042	0.10	N/A
12	1.0	0.083	1.66	0.76 ± 0.022
12	1.5	0.125	8.59	N/A
12	2.0	0.167	27.21	N/A
15	0.5	0.033	0.04	N/A
15	1.0	0.067	0.67	0.27 ± 0.007
15	1.5	0.100	3.47	N/A
15	2.0	0.133	11.10	N/A
20	0.5	0.025	0.012	N/A
20	1.0	0.0500	0.209	0.80 ± 0.004
20	1.5	0.075	1.076	N/A
20	2	0.100	3.45	N/A

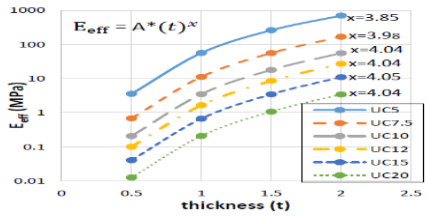

FEA calculated effective modulus vs element thickness *(t)*

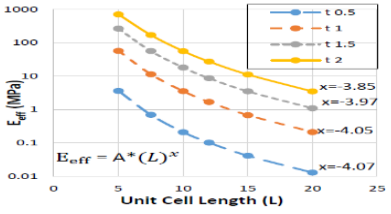

FEA calculated effective modulus vs unit cell length *(L)*

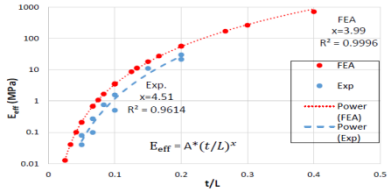

FEA calculated effective modulus of diamond lattice vs (*t/L*) compared to experimentally-measured effective modulus values and designed (*t/L*).

The stiffness of the LS components measured from the compression test data is summarized in Table 1 and presented on Figure 3.13 and Figure 3.14 . Only the unit cell size of 10 mm has sufficient points to fit a relationship to effective modulus (Figure 3.13). It has an exponent significantly higher than predicted by the FEA (4.8). The experimental relationship with unit cell size is much closer to the FEA results with exponent of 3.7 and 4.02 for 0.5 mm and 1.0mm element sizes respectively. It is also noted from Figure 3.13 and Figure 3.14 that the effective modulus measured experimentally is substantially below the FEA predictions for all the tests cases though the difference is reduced at larger element size (*t*) values. This may be explained by the surface characteristics of LS components.

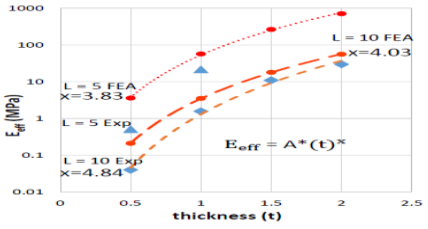

FEA vs experimental values of the effective lattice modulus vs element thickness *(t)*

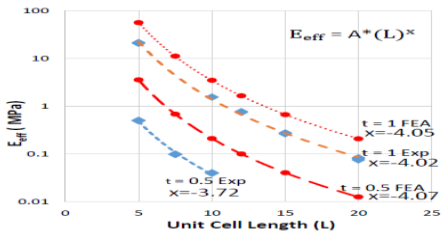

Comparison of FEA simulated to experimentally measured effective modulus vs unit cell length *(L)*

Laser sintered PA 2200 generally leaves partially densified layers on the outer surface of the part geometry that contributes to weight and thickness measurements, but does not influence strength and stiffness characteristics. This means that a designed part may not have the designed strength and stiffness intended because the measured thickness is not fully supporting the part geometry. Figure 3.15 below is an SEM image of the surface of a LS part cleaned with compressed air that illustrates the lightly compacted layers and surface roughness of laser sintered PA 2200.

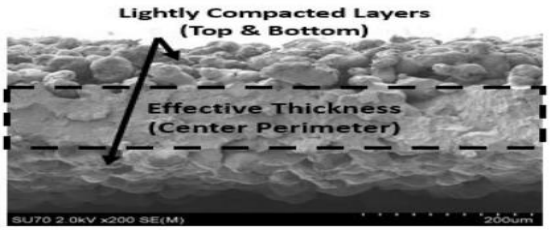

SEM image of laser sintered PA 2200 fracture surface illustrating surface structure of a single laser pass after air cleaning

These partially densified surface structures would substantially decrease the effective modulus of the thin printed elements to create a lower experimental measurements of effective modulus. Further, a consistent low density surface layer would have a larger impact on the thinner components and could produce the larger errors observed in the thinner element sizes. In order to further evaluate this possibility, the effective element size of each experimental element that would give the measured modulus values was calculated by scaling the FEA predictions based on the fourth order power relationship observed above.

The effective element size calculated for each experimental condition is summarized in Table 2. It is noted that the difference between the designed thickness and the effective thickness varies between 0.184 and 0.317 mm with an average of 0.211 mm for the variety of diamond lattices printed. The difference remains consistent across feature sizes from 0.5 mm to 1.5 mm. The lightly compacted layers for laser

sintered parts directly effects the performance of the diamond lattices in relation to the elastic modulus. Table 2 indicates 0.5 mm thickness lattices have the largest difference of FEA to experimental elastic modulus and this is explained because the 0.211 mm effective thickness error is a much greater percentage of 35 – 41 % of designed thickness. As the thickness increases, the lightly compacted layers contribute to less of the designed thickness (close to 20%), thus reducing the divergence between experimental and simulated results.

Table 2: Effective thickness evaluation for FEA and experimental modulus deviation

Unit Cell Length *(L)*	Thickness *(t)*	Effective Thickness Error	Percentage of Designed Thickness	$\frac{E_{FEA}}{E_{exp.}}$
5.0	0.5	0.204	41%	7.11
7.5	0.5	0.202	40%	6.94
10	0.5	0.177	35%	5.12
5.0	1.0	0.228	23%	2.66
10	1.0	0.193	19%	2.25
12	1.0	0.187	19%	2.29
15	1.0	0.213	21%	2.47
20	1.0	0.225	23%	2.63
10	1.5	0.184	12%	1.64
10	2.0	0.307	15%	1.88

Given the consistent magnitude of the difference between the design and effective thickness values, this could be applied as a design offset. The average of the effective thickness error calculated for all parts was subtracted from the design thickness to calculate an effective thickness. The effective modulus results are reported in Figure 3.16.Since now the effective thickness is being applied for experimental results, the points are essentially shifted and promptly coincides to an enhanced resemblance to the numerical simulations. The substantially improved agreement between FEA and experimental measurements with this correction suggests that this is an easy way to compensate for the process effects on material stiffness when designing for a target stiffness level.

In practice, there may be additional sources of error including variations in material properties with thickness and errors in unit cell size, but these factors are unlikely to cause the large differences in experimental modulus values observed since unit cell size errors are much smaller and the lattice modulus value varies only linearly with material modulus of elasticity. Figure 3.17 plots the experimental and FEA modulus values against the (*t/L*) ratio, but utilizes the adjusted thickness values (design thickness minus average thickness error) for the experimental values. With this adjustment, the experimental and FEA results show good agreement. Careful assessment of these other error sources may yield further improvements in the prediction of lattice properties to guide design.

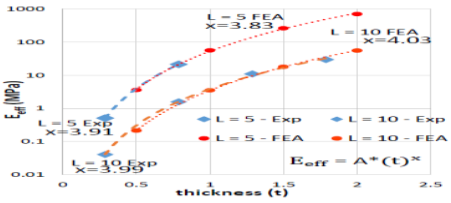

Comparison of effective lattice modulus predicted by FEA simulation vs experimental modulus measurements vs utilizing corrected thickness (t) values

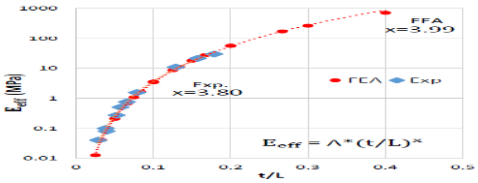

Simulation and experimental values of the effective elastic modulus measurements vs (*t/L*) utilizing the corrected thickness *(t)* values

DESIGN SPACE AND SCALING OF LATTICES RESEARCHED

As mentioned above, different combinations of thickness and unit cell length that produce the same *(t/L)* ratio for the diamond lattice configuration will have constant effective modulus and density values. Figure 3.18 presents a chart that can identify potential unit cell length and thickness for given stiffness and density. Along the dark lines are FEA values that are then extrapolated (dashed lines) to expand the amount of design space for diamond lattice parameters. The shaded triangular region is where the relative density limit of 30% is drawn as in that region design start to diverge from the realm of cellular solids. Additional limits are imposed by the process resolution constraints. The minimum

thickness is the minimum feature size of the part—here taken as 0.5 mm. Within this region, *t/L* values can be selected to achieve the desired effective modulus values.

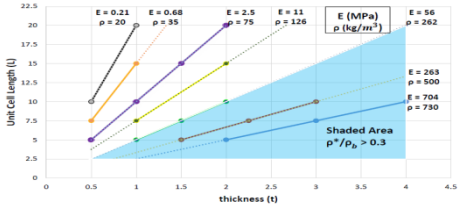

Plot of constant curvature/density lines as a function of unit cell and thickness dimensions

Meta-structured systems can create an effective "meta-material" with properties that can be tuned to specific design requirements. Generating meta-materials in the arrangement of diamond lattice has proven to produce structures that vary in effective elastic modulus over four orders of magnitude (shown in Figure 3.17). The stiffness is shown to vary to the fourth power with the ratio of the element thickness to the unit cell size. This research also provides an effective error analysis for the thickness of laser sintered parts to assess the divergence of simulated and 40 experimental results. Once an effective thickness was applied, the experimental results were in agreement with FEA.

IV. MODIFICATION OF DIAMOND LATTICE PARAMETERS TO EXPAND RANGE OF MECHANICAL PROPERTIES AND POISSON'S RATIO EVALUATION

It explores modifying diamond lattice parameters other than unit cell length *(L)* and thickness *(t)*. By modifying different build parameters diamond lattice properties are further evaluated to expand the range of attainable properties in the previous chapter. This chapter also provides analysis for Poisson's ratio of diamond lattices.

SCALING DIAMOND LATTICE PROPERTIES INTO OTHER MATERIALS AND ASHBY CHARTS

This research establishes a well-defined effective stiffness and density range for diamond lattices constructed of PA 2200 as the material. PA 2200 manages to range across 5 orders of magnitude for stiffness and reaching stiffness and density values of 56 MPa and 262 kg/m^3 respectively-employing the relative density limit of 30%. These values are meaningful but during research it was thought: how can we extend the range of properties attainable without changing build parameters besides thickness and unit cell length? The answer resides in scaling the diamond lattices into other materials other thanNylon.

Scaling diamond lattice values into other materials of: other thermoplastics like ABS (Acrylonitrile butadiene styrene), PLA (Polylactic acid); and especially metals of: Steel, Titanium, and Aluminum were of particular interest as alternate materials and commonly 3D printed. To obtain the correct scaling values for effective stiffness and density the relative stiffness and density was utilized. The relationship between relative stiffness and density according to thickness and unit cell length has already been acquired through the prior analysis of this research. By equating the known relative stiffness and density values for Nylon (PA 2200) to another relative value for another material we can calculate the effective stiffness and density values. Equation 11 and Equation 12 below show the equated relationship for relative stiffness and density.

$$\left(\frac{E^*}{E_{bulk}}\right)_{Nylon} = \left(\frac{E^*}{E_{bulk}}\right)_{Alt.Matrl} \qquad \text{Equation 11}$$

$$\left(\frac{\rho^*}{\rho_{bulk}}\right)_{Nylon} = \left(\frac{\rho^*}{\rho_{bulk}}\right)_{Alt.Matrl} \qquad \text{Equation 12}$$

To calculate the effective stiffness and density value for another material simply multiply the relative stiffness or density by the bulk property of an alternate material. Table 3 presents the bulk material properties used to calculate effective stiffnesses and densities for alternate materials. This method will reveal effecttive stiffness and density values according to thickness and unit cell length for the alternate materials in Table 3.

Table 3: Bulk material properties

Material	Bulk Modulus - E_{bulk} (GPa)	Bulk Density - ρ_{bulk} (kg/m^3)
Nylon	1.7	930
ABS	2.0	1020
PLA	3.3	1250
Steel	200	7900
Ti	120	4650
Al	69	2700

Figure 4.1 (also employing the realtive density limit of 30%) below shows the plots of calculated effective stiffness versus *t/L* for different materials and shows a drastic change in the range of stiffness attainable for diamond lattices. Contrasting ABS to steel, results signify an increase in stiffness from 56 MPa to 7 GPa, or 12,400% increase. The massive increase in the stiffness comes from the fact of the bulk stiffness of the steel and other metal is much higher than Nylon (PA 2200). As for the thermoplastics of ABS and PLA, stiffness was relatively similar because the bulk stiffness is on the same order of magnitude as Nylon (PA 2200). Figure 4.2 directly compares the stiffness and density for the metal materials also including *t/L* values. Figure 4.2 interprets the steel will have the stiffest lattice but also the highest density for a given *t/L*. The metal lattices add apporximately another two orders of magnitude for stiffness attainable.

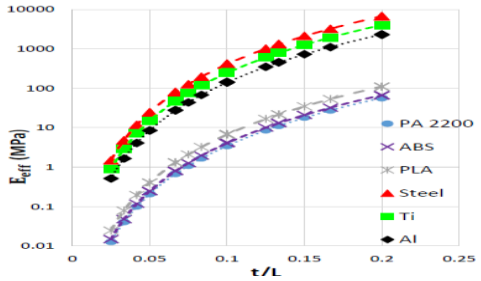

Effective stiffness vs *t/L* for different materials

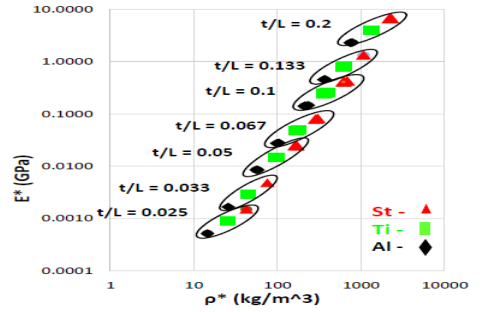

Effective stiffness vs effective density for metal diamond lattices

Extending diamond lattices into metals also increases the design space vastly. Section 2.4 introduces the potential design space lattice structures could fill. When the diamond lattice analysis includes metal materials, overlaid material property charts below illustrate the design space fulfilled by diamond lattices. Analyzing the diamond lattice overlay onto the material property chart of Figure 4.3 the diamond lattice materials fit well into the porous solids domain region. Figure 4.4 displays a direct comparison of diamond lattices to other recently researched lattice structures. It should be noted Figure 4.4 terms other "lattice" structures. These lattices were stretch dominated lattice configuration so the reason for higher stiffness to weight ratios. Remember stretch dominated lattices seek to optimize specific stiffness unlike bending dominated structures operating in the low stiffness bending regime.

Both material property charts below show metal diamond lattices fit well to metal foams and also into regions of solid natural materials and engineering polymers. This is analogous to the cellular metal diamond lattice having the same stiffness and density as a "solid" natural material or polymer. A diamond lattice structure having the ability to mimic stiffness of a solid polymer drives multi-functionality. Since the diamond lattice is not a solid material but cellular and porous, it provides be flexibility and compliancy at the same stiffness as a solid material. The porosity also reduces the amount of material thus generating a lightweight structure. As previously mentioned, the property of compliancy pertaining to a diamond lattice yields an energy absorbent structure. The porous structure also allows for a convective fluid to pass through allowing a potential cooling or heating effect. Thus, instead of a solid material as structural members, diamond lattices provide the same stiffness capable of multiple functions. This realization proves the design space for diamond lattices as lightweight, multifunctional, load bearing structures to potentially replace solid structural material.

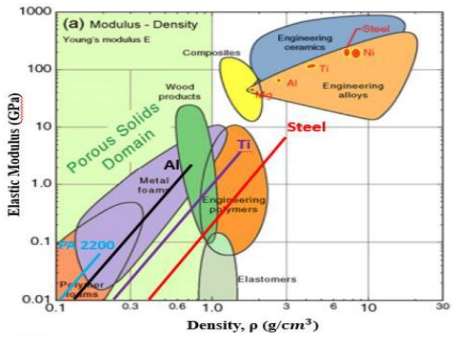

Modulus vs density material property chart for porous, cellular solids

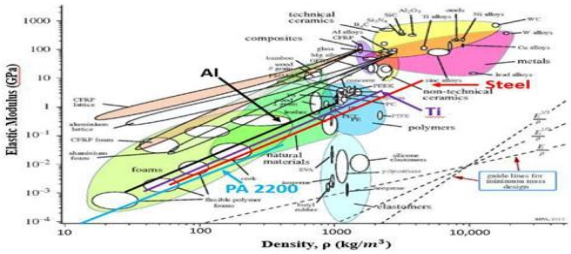

Overlaid material property chart encompassing design space of lattice structures

DOUBLE ARC CONFIGURATION

The previous section presents deviation from the *(t/L)* curve and filling the design space of diamond lattice properties, but how could diamond lattice stiffness be enhanced to increased values of stiffness for the same density? One modification to diamond lattices creates double arcs for struts. Double arc (DA) diamond lattices essentially creates a circular arc of uniform thickness where a single strut existed in the standard (St.) diamond lattices. Figure 4.5 illustrates a diamond lattice with double arc configuration. The radius of curvature was set in order to intersect the joining nodes an individual arc strut connects. To connect the joining nodes, the radius of curvature relates to unit cell length *(L)* by: *(radius = 0.433*L).* Double arc simulations were analyzed for strut thickness *(t)* for the different unit cell length *(L)* in Table 4. It is hypothesized that creating a double arc would increase stiffness-but would there be tradeoffs with the increase in stiffness?

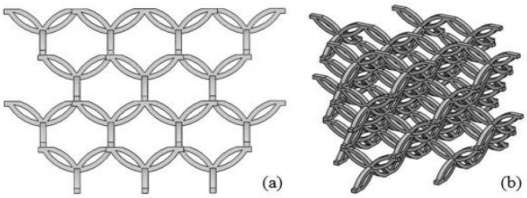

Diamond lattice double arc (DA) front view (a) and isometric view (b)

Figure 4.6 and Table 4 double arcs display an increase in stiffness from 2.5 – 3 times the stiffness of the standard diamond lattice. This confirms the hypothesis of increase stiffness but the double arcs also increase the density of an individual diamond lattice. Density for a double arc is 1.6 – 2 times a standard diamond lattice. Approximately double the density falls logically with the reasoning a double arc will basically have a double strut for a given thickness *(t)* instead of a single strut for a standard diamond lattice.

Another aspect comparing double arcs and standard diamond lattices is the exponents of Figure 4.6 and Figure 4.7. Inspecting the charts show the double arcs have a higher exponent than the standard diamond lattices. A higher exponent implies different scaling of stiffness with the unit cell and density parameters. This is seen in Figure 4.7 as a decrease in the distance between the stiffness off the single and double arc at higher density values.

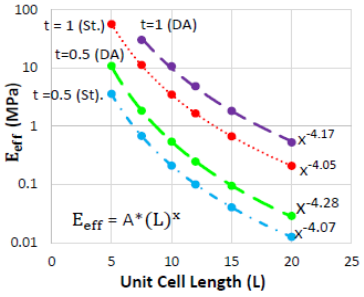

Diamond lattice double arc and standard effective stiffness vs unit cell length *(L)*

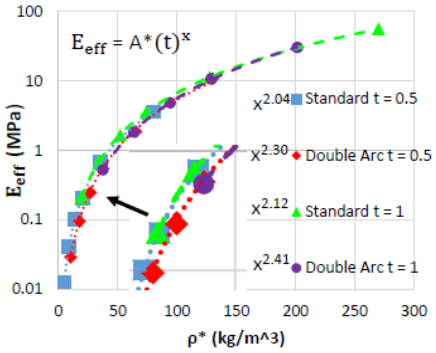

Diamond lattice double arc and standard effective stiffness vs effective density

Table 4: Ratio of double and standard diamond lattice stiffness and density

Unit Cell Length *(L)*	Thickness *(t)*	*t/L*	$\frac{E_{double}}{E_{standard}}$	$\frac{\rho_{double}}{\rho_{standard}}$
5.0	0.5	0.100	3.02	1.63
5.0	1.0	0.200	N/A	N/A
7.5	0.5	0.067	2.71	1.83
7.5	1.0	0.130	2.70	1.58
10	0.5	0.050	2.58	1.88
10	1.0	0.100	3.05	1.75
12	0.5	0.042	2.46	1.95
12	1.0	0.083	2.92	1.81
15	0.5	0.033	2.34	1.96
15	1.0	0.067	2.75	1.88
20	0.5	0.025	2.40	2.00
20	1.0	0.050	2.53	1.93

EVALUATION OF POISSON'S RATIO

Since the diamond lattices design intent is a bending dominated structure, this research hypothesizes a relatively high positive Poisson's ratio. The ratio between lateral to axial strain induced during uniaxial loading of a material or structure defines Poisson's ratio *(υ)*.

Materials with a positive Poisson's value under compressive loading will contract in the loading direction and expand in the orthogonal (lateral) directions. When a material is placed in a state of tension it will stretch in the direction of applied load and contract in orthogonal directions. The limit for most isotropic material is a positive Poisson's ratio of $\upsilon = 0.5$; however, structures built with the intent of very high shear strain can breach the isotropic limit. Negative Poisson's or "auxetic structures" ratios behave exactly opposite of its positive counterpart and have a limit of υ=-1. More information on auxetic structures can be found from the research by Zhang, Soman, and Alderson. For diamond lattices we concentrate on compressive loading conditions. Compression in the axial direction causes the axial strain to equal Equation 13 where Figure 4.8 defines (Δuz) as the change in length upon compression and (ho) as the initial length of the diamond lattice.

$$\varepsilon_{axial} = \frac{\Delta u_z}{h_o} \qquad \text{Equation 13}$$

As mentioned above as a compressive load applies axially to a structure it will expand in the lateral direction. This expansion causes a lateral strain. The lateral strain is prescribed in Equation 14. Since the expansion is lateral as seen in Figure 4.8, the width of the lattice is now defining the lateral strain by (Δux) designating the horizontal displacement of each side when compressed (the expansion) and (w_o) nominating the original width of the lattice. The change in width is the expansion on the outside edges in the horizontal direction for both sides of the lattice.

$$\varepsilon_{lateral} = \frac{2\Delta u_x}{u_o} \qquad \text{Equation 14}$$

After calculating both the axial and lateral strains, Poisson's ratio can be found. Equation 15 shows the relationship of the lateral strain divided by the axial strain to equal Poisson's ratio *(υ)*.

$$\upsilon = \frac{-\varepsilon_{lateral}}{\varepsilon_{axial}} \qquad \text{Equation 15}$$

Evaluation of Poisson's ratio for diamond lattice entailed the same simulation method as the stiffness extraction. A linear study for 1% strain was applied axially ($\varepsilon axial$) to different combinations of *(t/L)* values. After the simulation completed the measurement of Δw was extracted to find the lateral strain ($\varepsilon lateral$). Once the lateral strain was calculated the Poisson's ratio was found.

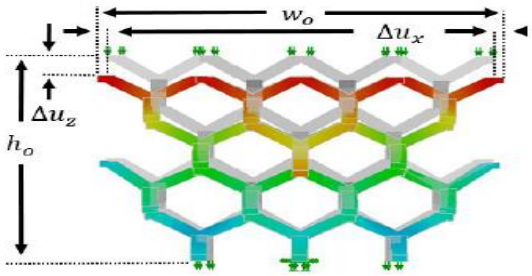

Elongation in axial and transverse directions for Poisson's ratio

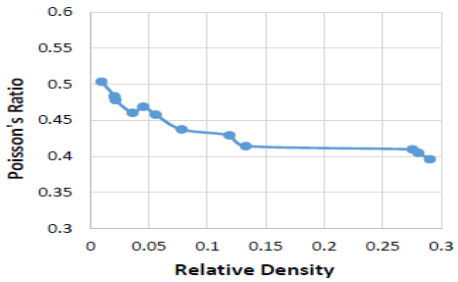

Poisson's ratio for diamond lattices

Figure 4.9 indicates Poisson's ratio for different relative densities. At low relative densities Poisson's ratio is close to 0.5 and decays in decreasing value to ~0.4 as the relative density approaches the cellular solid limit of 30%. A value of 0.5 for Poisson's ratio is the maximum an isotropic material can achieve and only structures designed for high shear can pass the 0.5 limit.

Most metals have Poisson's ratio of 0.3 ±0.0.5, polymers ~0.4, and rubber (0.48) being the only material approaching the limit of Poisson's ratio. [54] The diamond lattices ability to reach Poisson's ratio of 0.5 is interesting as it places the structure near the max and above most materials and structures.

A value of 0.5 for Poisson's ratio of isotropic materials means the material is incompressible. A near incompressible material-like rubber or water- does not allow compressibility and volume is conserved. [55, 56] A great application for rubber is O-rings and sealants. For O-rings and sealants volume conservation is desired because when an O-ring or sealant is compressed, the volume of material expands in the lateral direction thus creating a seal for the mated parts. A diamond lattice close to a value of 0.5 for Poisson's ratio will approach incompressibility. If applications require large expansion in the lateral direction, diamond lattices could fulfill this requirement.

The reasoning why the Poisson's ratio decays as the relative density increases for diamond lattice resides in the struts becoming relatively thicker. As either the thickness *(t)* increases or the unit cell length *(L)* decreases the relative density increases because the struts are increasing in relative thickness for the diamond lattice. With the struts increasing in relative thickness, Euler beams become less accurate. Slender struts promote bending so a low relative density diamond lattice will closely approach the theoretical limit of isotropic, solid materials for Poisson's ratio of 0.5.

V. CONCLUSIONS AND FUTURE WORK

This thesis explored the design space for low stiffness, bending dominated structures in the form of diamond lattice configuration. Diamond lattices exemplify a bending dominated structure because of the obtuse angles of its strut members and the lower number of connections of struts at the joints. The wide sweeping angles allow for the structure to bend when a compressive load is applied. This chapter begins with reiterating the motivation for this thesis. Concluding analysis follows the motivation in terms of experimental versus FEA data and also modifications of the diamond lattice parameters for expansion of properties.

5.1 MOTIVATION AND THESIS GOALS

The goal of this thesis is to evaluate diamond lattice mechanical properties (specifically stiffness and density) to fulfill meta-material design space. Previous work focused on maximizing the specific stiffness in the meta-material design space. Maximizing specific stiffness uses reinforced geometry to enhance the stiffness and strength of a lattice structure; but these same reinforcements prevent bending of the struts. With bending prevented, strains are small and energy absorption is sacrificed. This is where the potential for diamond

lattices becomes valuable in the realm of low stiffness, energy absorbent structures. This thesis is successful in documenting the range of effective stiffness that can be reached by diamond lattices for potential use in energy absorbent applications.

EXPERIMENTAL VERSUS FEA ANALYSIS

Chapter two's central theme describes the foundation of cellular solids by detailing how the governing principles will promote a cellular lattice structure response. Much of the chapter focused on the derivation and description of bending-dominated structures and to display the design space available. Chapter three validates the relations derived in chapter 2 both experimental and simulated. At first, experimental and simulation data entailed a discrepancy to not fully agree. Further analysis ensued to explain the discrepancy and was found in analyzing the effective thickness of laser sintered diamond lattices.

Laser sintering my leave behind lightly compacted layers on the outer surface of a part's geometry. In the case of the diamond lattices, the lightly compacted layers changes the effective thickness of the struts *(t)*. The lightly compacted layers on the outer surface of the struts essentially made the diamond lattice struts respond thinner than expected by a constant amount that was independent of the total strut size. The lightly compacted layers contribute to weight and thickness measurements but do not increase the mechanical response of the diamond lattice. Lightly compacted layers constitute a larger percentage of the strut thickness for smaller strut sizes therefore these elements deviate farther from predictions. A thickness correction was applied to the experimental data to find an effective thickness of the laser sintered diamond lattices; once applied the experimental data shifted to be in agreeance well with simulated data.

After correction, both experimental and simulated data proved the relationship of the diamond lattices build parameters to effective stiffness and effective density to hold true for a structure in the bending dominated regime. From chapter two's derivations, bending dominated structures relate relative density to a squared *(t/L)* relationship (Equation 2). Since relative stiffness derives a squared relationship of relative density (Equation 5), build parameters thickness *(t)* and unit cell length *(L)* are proportional to effective stiffness to the fourth power (Equation 6). The fourth power relationship is consistently shown in the charts of chapter 3 and confirms diamond lattices are indeed bending dominated structures. Chapter 3 also shows that diamond lattices constructed of PA 2200 can tune stiffness range over four orders to magnitude. Four orders of magnitude is a significant portion of design space for a wide range of applications for low stiffness.

RECOMMENDATIONS FOR FUTURE WORK

Future work for diamond lattices considers further exploration for isotropy. Confirming the diamond lattice is isotropic is valuable as it means the diamond lattice would have the same mechanical response in all directions. Having the same stiffness reaction in the longitudinal and lateral directions generates a structure that can be loaded regardless of direction.

Other work can be done evaluating different loading conditions placed on diamond lattices. Shear forces when placing the diamond lattice into a sandwich structure are an interesting aspect that needs work done. All of the experiments and simulations of the diamond lattices were completed with uniaxial loading, but what would happen if the diamond lattices was placed in a state of biaxial or even multiaxial loading? Research could be done with other loading conditions to analyze the complicity of the stiffness reaction.

Another central aspect for further research lies in quantifying the energy absorbance the low stiffness structures. Completing experimental fatigue tests with cyclic loading can evaluate how much energy will be absorbed when repeatedly loaded. Energy absorption of diamond lattices would be valuable to quantify as this research has already proven a range of

tunable stiffness that could tuned even further for specific energy absorbent applications.

Lastly, while this research proves diamond lattices fill design space gaps in meta-material space, more work can be done on lattice structures that can fill even more design space-specifically different areas on the material property charts of chapter 4. Further research could be done in modifying the diamond lattice by changing the angles of the joining struts or maybe reinforcing the diamond lattice in strategic points where deformation is highest. Modifying the diamond lattice or even analyzing other lattice structures could fill more design space and open up many more applications for lattice structures.

VI. REFERENCES

[1]. Ashby, M.F., The Mechanical Properties of Cellular Solids. Metallurgical Transactions A, 1983. 14A.

[2]. Elliot, J.C., Method of producing metal foam, in U.S. Patent No 2,751,289. 1956.

[3]. Engelbrecht, S.S., Design of Meso-Scale Cellular Structure for Rapid Manufacturing, in Mechanical Engineering. 2009, Georgia Institute of Technology. p. 175.

[4]. Luis Folgar, D.W.R., Gary Schulberger, Jim Williams, Cellular structures for optimal performace, in 20th Annual International Solid Freeform Fabrication Symposium, SFF. 2009: Austin, TX. p. 831-842.

[5]. Gebhardt, A., Understanding Additive Manufacturing. 2012: Carl Hanser Verlag.

[6]. I. Gibson, D.W.R., B. Stucker, Additive ManufacturingTechnologies: Rapid Prototyping to Direct Digital Manufacturing. 2010, New York: Springer.

[7]. Tie Jun Cui, D.S., Rupeng Liu, Metamaterials Theory, Design, and Applications. 2010: Springer. 367.

[8]. Jane Chu, S.E., Greg Graf, David W. Rosen, A comparison of synthesis methods for cellular structures with application to additive manufacturing. Rapid Prototyping Journal, 2010. 16 (4): p. 275-83

[9]. D. M. Watts, R.J.H., Exploring the design freedom of RM, in Proceeding of the 17th International Solid Freeform Fabrication (SFF) Symposium. 2006: Austin, TX.

[10]. Rosen, D.W., Design for additive manufacturing: a method to explore unexplored regions of the design space, in Proceedings of the 18th International Solid Freeform Fabrication (SFF) Symposium. 2007: Austin, TX.

[11]. J. Schwerdtfeger, P.H., R. F. Singer, C. Korner, Auxetic cellular structures through selective electron-beam melting. Physics Status Solidi 2010. 247(2): p. 269-272.

Cite this article as :

S. Lingamaiah, "Investigative Analysis on Mechanical Properties of Laser-Sintered-Nylon Diamond Lattices", International Journal of Scientific Research in Science and Technology (IJSRST), Online ISSN : 2395-602X, Print ISSN : 2395-6011, Volume 8 Issue 6, pp. 178-199, November-December 2021.

Journal URL : https://ijsrst.com/IJSRST218610